

Topical Editor Decision: Publish subject to minor revisions (review by editor) (05 Oct 2018) by Marc Salzmann

Comments to the Author:

Thank you very much for submitting a revised manuscript. We received one reviewer report which you can find below. I agree with this report. Further revisions are necessary before your manuscript can be published. Because the overall assessment of your manuscript by the reviewers has been positive, I strongly encourage you to revise your manuscript based on the suggestions in this report.

Dear Editor: Really, really thank you very much for your kindly comments and suggestions. We have followed your suggestions and the reviewer's comments and the corresponding revisions have been made. The changes we made are shown in red font. The revised manuscript with tracked changes is attached later.

Reviewer Report #1:

The authors have responded to most of my minor comments in a satisfactory manner. However, some critical issues prevent the manuscript from being published in its present form, as detailed in the following.

General concern:

The response to my general concern is not clear enough, which also means that the motivation for the analysis of tropopause ascent (rather than tropopause drops) is not outlined well in the manuscript itself. In many of the cases in the manuscript, as well as in Hocker et al 2007, the intrusions are associated with a drop+ascent of the tropopause. I do not fully understand the reference to other atmospheric processes in the response, or how it supports the argument that the intrusions are not related to tropopause drops. Especially the following sentence is unclear: "In other words, various atmospheric processes (and the accompanied tropopause drops) are important conditions for intrusions (or for the strong downdrafts in our study), but intrusion events are not close related to tropopause drops". It is also very confusing to note in the response that the intrusions and the downdrafts are the same thing, while in other places

it is mentioned that the downdrafts precede the tropopause ascent and the intrusions. Therefore, a clear distinction of the terms should be made early on in the introduction. In addition, the word “predictor” should be replaced by “diagnostic”, for example as it appears in the response “Therefore, we think the strong downdrafts just preceding the rapid tropopause ascent (black bands shown in Fig.13) may serve as a valuable predictor for possible stratospheric intrusions” and in the revised manuscript in line 265 to avoid such confusion. I suggest that the authors revise this part of the text, to convey their motivation better, including English language editing. This issue seems to arise also from the comments of referee #2, and the editor, and deserves careful attention.

Response: Really thank the reviewer for the comments. Firstly, we must admit that we cannot conclude that the intrusions are not related to tropopause drops at all. It is from the perspective of quantifying intrusion events that the choice of tropopause ascent (with specific erosion velocity) is more reasonable and feasible than the choice of tropopause drops. This is evidenced by the actual high-resolution observations: (especially with the unique high temporal resolution ozonesonde soundings) by Hocking et al., (2007). The observation results clearly indicate that almost every occurrence of definite stratospheric intrusion is related to a definite RT ascent (>0.2 km/h, occurred at or just before the intrusion). The reverse is also true, that is almost every occurrence of definite RT ascent is associated with some form of intrusions. Therefore, as motivated by this study, tropopause ascent is one of the objects in our manuscript. Please noted that we also cannot conclude that the tropopause ascent is the best and accurate signature that can be used directly for identifying possible intrusions. Therefore, the vertical wind velocity features have also been taken into account in our study. To convey our motivation better, the corresponding sentences in the introduction have been modified, please see the sentences: **‘The research by Hocking et al., (2007) have achieved a development in this issue and reported that the rapid ascent in RT altitude (>0.2 km/h) can be a valuable diagnostic for possible stratospheric intrusions. Their observation results clearly indicate that almost every occurrence of definite stratospheric intrusion is related to a definite RT ascent (>0.2 km/h, occurred at or just before the intrusion). The reverse is also true, that is almost**

every occurrence of definite RT ascent is associated with some form of intrusions. Please noted that we did not mean that the tropopause ascent is the best and most accurate diagnostic that can be used directly for identifying possible intrusions. As motivated by the study of Hocking et al., (2007), tropopause ascent is one of the key objects in this study.'

Very, very sorry for the confusing response. The vertical motions (downdrafts) and the downward intrusions are not the same thing. To make relationship between the three terms (tropopause ascent, downdrafts, and intrusions) been described clearer, the corresponding sentences in the introduction section have been modified, please see the sentences in the present revised manuscript: **'Using only the information of RT height variability is, of course, insufficient for quantifying intrusion events accurately by radar data. Therefore, radar measurements of vertical motions here are also considered simultaneously to discuss the possible capability of radar measurements for identifying cross-tropopause stratospheric intrusions, which is the main point of this paper. This study is carried out mainly via a detailed case observation during a COL passage and other 20 general cases during various synoptic processes.'**

I'm very sorry about inaccurate use of the word "predictor". In fact, the "predictor" has already been replaced by "diagnostic" in the revised manuscript uploaded in 30 Aug. 2018. Please see the sentence in the present revised manuscript: **'The research by Hocking et al., (2007) have achieved a development in this issue and reported that the rapid ascent in RT altitude (>0.2 km/h) can be a valuable diagnostic for possible stratospheric intrusions'.**

Specific major comments:

2. In the revised manuscript you still state on lines 311-312:"Trajectory results further support the evidence of possible stratospheric intrusions that closely related with the

main downdrafts”, even though the authors agree that this is not supported by the trajectory analysis.

Response:

I'm so sorry. In order to avoid misleading potential readers, the corresponding sentence has been modified to **'Trajectory results further support the evidence of downward intrusions that closely related with the main downdrafts.'**

Specific minor comments:

1. Please enhance and edit the English, as for the general concern above.

Comments 7 and 9: The high-PV at mid levels is not accompanied by high ozone according to Fig. 8. Therefore, it is probable that this is not a major stratospheric intrusion, but rather a diabatically-produced high PV, or a different kind of advection of high PV, but not a clear stratospheric intrusion. This is especially true because the existence of stratospheric intrusions is not supported by the trajectory analysis. This issue is not addressed in the revised manuscript as it should.

Response: Really, really thank the reviewer for the valuable comments. According to Figure 8, the high-PV and dry air have been observed intruding deep into troposphere of ~650 hPa. Whereas the vertical structure of AIRS ozone has shown that the enhanced ozone intruded into troposphere of ~500 hPa. From this figure, one thing is clear that stratospheric air (characterized by dry ozone-rich and high-PV) intrusions are indeed occurred and observed (at least deep into 500 hPa). This difference in vertical scale of intrusion between ozone and PV parameters is most likely due to two reasons: 1) the local high PV value observed at ~600 hPa is not a true stratospheric characterized intrusion but rather a diabatically-produced high PV (e.g. Škerlak et al 2015); 2) the relatively poor vertical resolution of AIRS ozone data may have limited the refined observation of the intrusions. In order to make this issue be addressed clearer, the second paragraph of section 3.3 have been modified substantially. Please the sentences in the revised manuscript: **'Please note that the high-PV and dry air have been observed intruding deep into troposphere of as low as 650 hPa (~3.6 km). Whereas the vertical structure of AIRS ozone has shown that the enhanced ozone intruded**

into troposphere of ~500 hPa. This difference in vertical scale of intrusion between ozone and PV parameters is most likely due to two reasons: 1) the local high PV value observed near ~600 hPa is not a true stratospheric characterized intrusion but rather adiabatically-produced high PV (e.g. Skerlak et al 2015); 2) the relatively poor vertical resolution of AIRS ozone data may have limited the refined observation of the intrusions. From this figure, however, one thing is clear that stratospheric air (dry ozone-rich and high PV) intrusions are indeed occurred and observed (at least deep into 500 hPa).'

1 **Strong downdrafts preceding rapid tropopause ascent and their potential to**
2 **identify cross-tropopause stratospheric intrusions**

3 Feilong Chen¹, Gang Chen^{1*}, Chunhua Shi², Yufang Tian³, Shaodong Zhang¹,
4 Kaiming Huang¹

5 ¹School of Electronic Information, Wuhan University, Wuhan 430072, China.

6 ²Key Laboratory of Meteorological Disaster, Ministry of Education, Nanjing
7 University of Information Science & Technology, Nanjing 210044, China.

8 ³Key Laboratory of Middle Atmosphere and Global Environment Observation,
9 Institute of Atmospheric Physics, Chinese Academy of Sciences, Beijing 100029,
10 China

11 *Corresponding author: Gang Chen (g.chen@whu.edu.cn)

12
13 **Abstract:**

14 The capability of measuring 3-dimensional wind and tropopause structure with
15 relatively high time and vertical resolution makes VHF radar a potentially significant
16 tool for studying various processes of the atmosphere. In the light of present
17 understanding, using VHF radars to identify possible stratospheric intrusions still
18 remain unclear. Here the potential detection of stratospheric intrusion events is
19 discussed using the Beijing MST radar located at Xianghe (39.75°N, 116.96°E). During
20 the passage of a cut-off low in late November 2014, a deep V-shaped tropopause
21 structure, and strong downdrafts (>0.8 m/s) immediately preceding the rapid tropopause
22 ascent (>0.2 km/h) were observed. Within the height region of the downdrafts, the

23 stability of the radar tropopause seems to be weakened. Analysis results from global
24 reanalysis and the satellite data, as well as the trajectory model have shown the clear
25 evidence of the downward stratospheric intrusions (dry ozone-rich and depleted
26 methane air) associated with the strong downdrafts. Twenty typical cases of such strong
27 downdrafts, occurring during various synoptic processes in different seasons, have been
28 presented and 15 of them are exactly associated with some form of stratospheric
29 intrusions. Four years (2012-2015) of such downdrafts are further discussed. The
30 observations reveal that the strong downdrafts preceding the rapid tropopause ascent
31 can be a valuable diagnostic for monitoring intrusion events, which will gain a better
32 understanding of stratospheric intrusions in VHF radar observations.

33

34 **Keywords:** Stratospheric intrusions; strong downdrafts; rapid tropopause ascent; MST
35 radar; VHF radar; cut-off low

36

37 **1. Introduction**

38 The tropopause is a stable transition zone separating the vertically stable stratified
39 stratosphere from the active free troposphere. The stratospheric and tropospheric air are
40 remarkably different in their chemical and dynamical characteristics. The stratosphere
41 is dominantly high in ozone and potential vorticity (PV) content and low in water vapor
42 (WV) and methane (CH₄) concentration, while the troposphere is just on the contrary
43 (Holton et al., 1995). Consequently, the natural stable tropopause layer, characterized
44 by strong gradients of trace constituents and wind speeds, plays an important role in
45 stratosphere-troposphere exchange (STE) processes. In other words, the layer is a
46 significant barrier for the atmospheric transport between stratosphere and troposphere
47 (Mahlman, 1997). From a long-term point of view, the seasonal variation of the
48 tropopause height determines the seasonal variation of the flux of stratospheric air into
49 the free troposphere (Appenzeller et al., 1996). Under the global climate warming (e.g.
50 the continuing rise in CO₂), the tropopause variation is also a significant factor that
51 must be considered with regards to the recovery of the stratospheric ozone (Butchart et
52 al., 2010; Chipperfield et al., 2017). On the other hand, the short-term tropopause
53 variability is sensitive to various meso- and small-scale atmospheric processes, during
54 which the folding/intrusion events commonly occur. This characteristic of the
55 tropopause change are sometimes directly used to detect the tropopause folds (e.g. Rao
56 et al., 2008; Alexander et al., 2012, and references therein), but are less, if any, directly
57 used to identify stratospheric intrusions. More detailed analysis of the variability of
58 high-resolution tropopause height and of course some other parameters (e.g. 3-

59 dimensional wind), and how the stratospheric air is transported across the tropopause
60 into the troposphere will help us to yield better understanding of the downward
61 stratospheric intrusions (e.g. Sprenger et al., 2003; Leclair de Bellevue et al., 2007; Das
62 et al., 2016).

63 Although photochemical production within the troposphere is the main source of
64 tropospheric ozone, the influence of downward stratospheric intrusions on tropospheric
65 ozone content cannot be ignored (Oltmans and Levy II, 1992; Stevenson et al., 2006).
66 Stratospheric intrusions bring dry ozone-rich air down into the free troposphere (e.g.
67 Stohl et al., 2000; Sørensen and Nielsen, 2001) and sometimes even deep to the surface
68 (e.g. Gerasopoulos et al., 2006; Grant et al., 2008; Jiang et al., 2015; Das et al., 2016;).
69 By now, it is well established that these intrusions of stratospheric origin will
70 significantly influence other trace gases (such as hydroxyl (OH)) in the troposphere
71 (Holton et al., 1995). These influences then will further contribute to the change of
72 radiative balance (Ramaswamy et al., 1992) and play an important role in the radiative
73 forcing of global climate change (Holton et al., 1995). It is true that stratospheric
74 intrusion events occur all over the world and in any seasons. However, they are highly
75 episodic in both vertical and isentropic (horizontal) directions (Chen, 1995). Various
76 dynamical and physical processes have been proposed to be responsible for extra-
77 tropical intrusion events. These mainly include tropopause folds, stratospheric
78 streamers and break-up, cut-off lows (COLs), wave breaking, and mesoscale convective
79 activities and thunderstorms (Stohl et al., 2003).

80 The certain dynamical and chemical characteristics of stratospheric air allow the

81 tracers, such as dry ozone-rich and high PV, to be proper indicators for the intrusions
82 penetrating down into the troposphere. Based on these tracers, various tools are
83 available to detect intrusion events. Balloon-borne ozonesonde sounding is an effective
84 tool to make measurements of ozone with high vertical resolution, but is limited by
85 coverage (He et al., 2011) and temporal resolution. In contrast, the satellite-borne
86 remote sensing instruments, such as Atmospheric Infrared Sounder (AIRS), can provide
87 nearly global coverage of various trace gases but have limitations in vertical and
88 temporal resolution. Another method for studying transport processes is trajectory
89 model, from which the backward trajectories can provide valuable information on the
90 possible sources of the trace gases (e.g. Elbern et al., 1997).

91 By far, large-scale STE has been widely studied and is fairly well understood, but
92 the details of small scale intrusions still need more researches (e.g. Holton et al., 1995).
93 Kumar and Uma (2009) reported that the shortage of direct measurements of vertical
94 winds near the tropopause may be responsible for the lack of fine-scale observations of
95 smaller scale intrusions.

96 Very-High-Frequency (VHF) radars, compared to the tools mentioned above, are
97 capable of continuously monitoring the atmosphere under any weather conditions and
98 detecting tropopause height from backscattered signal with both high temporal and
99 spatial resolution. During the past two decades, VHF radar measurements were
100 commonly used to assist to study the stratospheric intrusions (e.g. Hocking et al., 2007;
101 Das et al., 2016). However, it still remains uncertain in many aspects when using only
102 the VHF radar to identify intrusion events, especially the criteria for the identification.

103 Complicated and changeable atmospheric processes make it difficult to identify the
104 intrusion events by only radar data. The research by Hocking et al., (2007) have
105 achieved a development in this issue and reported that the rapid ascent in RT altitude
106 (>0.2 km/h) can be a valuable diagnostic for possible stratospheric intrusions. Their
107 observation results clearly indicate that almost every occurrence of definite
108 stratospheric intrusion is related to a definite RT ascent (>0.2 km/h, occurred at or just
109 before the intrusion). The reverse is also true, that is almost every occurrence of definite
110 RT ascent is associated with some form of intrusions. Please noted that we did not mean
111 that the tropopause ascent is the best and most accurate diagnostic that can be used
112 directly for identifying possible intrusions. As motivated by the study of Hocking et al.,
113 (2007), tropopause ascent is one of the key objects in this study.

114 Using only the information of RT height variability is, of course, insufficient for
115 quantifying intrusion events accurately by radar data. Therefore, radar measurements
116 of vertical motions are also considered simultaneously to discuss the possible capability
117 of radar measurements for identifying cross-tropopause stratospheric intrusions, which
118 is the main point of this paper. This study is carried out mainly via a detailed case
119 observation during a COL passage and other 20 general cases during various synoptic
120 processes. In section 2 the datasets used in this paper are described, section 3 presents
121 detailed results and discussion, and section 4 gives the conclusions.

122

123 2. Dataset

124 2.1. MST radar data and tropopause detection

125 The Beijing MST radar located at Xianghe, China (39.75° N, 116.96° E, 22 m
126 above sea level) is a VHF radar operated at 50 MHz and installed in 2010 based on the
127 first phase of Chinese Meridian Space Weather Monitoring Project (Chinese Meridian
128 Project for short) (Wang, 2010). The radar antenna array consists of 24×24 three-
129 element Yagi to produce an average power aperture product of 3.2×10⁸ Wm² and
130 maximum directive gain of 34.8 dB. It operates radiation pattern with 172 kW peak
131 power and 3.2° half-power beam width. More detailed information of the radar system
132 can be found in Chen et al. (2016). Routine low mode data were used for present study
133 with 0.5 h time resolution and 1 μs coded pulse, which provides 150 m vertical
134 resolution. Details of the low mode setup used in this study are given in Table 1.

135 It has long been known that VHF radar reflectivity is proportional to the mean
136 generalized refractive index gradient M , which is a function of humidity variation and
137 static stability and given by (Ottersten, 1969) as follows

$$138 M = -77.6 \times 10^{-6} (p/T) (d \ln \theta / dz) \\ 139 \cdot \{ 1 + 15500 q / T [1 - (d \ln q / dz) / (2 d \ln \theta / dz)] \} \quad (1)$$

140 where p is the atmospheric pressure (hPa) T is the temperature (K), θ is the potential
141 temperature (K) and q is the specific humidity (gg⁻¹). According to the second and third
142 terms of the equation (1): large humidity variation contributes to the echo from the
143 lower and middle troposphere. From the first term: the radar backscatter power is
144 proportional to the static stability, which in fact is directly proportional to the potential

145 temperature gradient. The tropopause, near which a strong potential temperature
146 gradient exists, will lead to strong radar echoes in vertical incidence, as well as large
147 radar aspect sensitivity (as shown in Figure 1). Radiosonde data used in this paper were
148 received from the GTS1 type digital radiosonde launched from Beijing Meteorological
149 Observatory (39.93 °N, 116.28 °E, station number 54511), which is less than 45 km
150 away from the MST radar site. The black line in Fig. 1 denotes the lapse-rate tropopause
151 (LRT) defined using the temperature lapse rate (World Meteorological Organization
152 (WMO), 1986). Applying the characteristic (enhanced radar echoes due to partial
153 specular reflection) mentioned above, the tropopause can be detected and its height
154 determined by VHF radars (Gage and Green, 1979). It has received widespread
155 application around the world, either in middle latitudes (e.g. Hocking et al., 2007), polar
156 regions (e.g. Alexander et al., 2012), and tropical regions (e.g. Yamamoto et al., 2003;
157 Das et al., 2008). Here, the radar-determined tropopause (RT) height is defined as the
158 height (above 500 hPa) where the maximum vertical gradient of echo power located
159 (shown as the orange circle in Figure 1a). This definition of RT is similar to that in the
160 studies of Alexander et al., [2012] and Ravindrababu et al., [2014].

161 In the present study, the MST radar mainly provides continuous measurements of
162 backscattered echo power, 3-D wind, and RT height with time resolution of 0.5 hour. In
163 addition, the radar aspect sensitivity, expressed as the ratio between vertical (p_v) and
164 oblique (p_o , here used the 15-degree north) beam echo power, is mainly caused by the
165 horizontally stratified anisotropic stable air and thus will be used as potential signature
166 of stratospheric intrusions in the troposphere (e.g. Kim et al., 2001). The backscattered

167 echo power given here is expressed as relative power in decibels (dB). In order to reduce
168 the random noise, the profile of p_v is smoothed by a 3-point running mean in altitude.
169 Note that the data that are heavily contaminated will be eliminated from our datasets.
170 The data of December 2015 and September 2015 are excluded.

171 2.2. AIRS satellite data

172 The AIRS instrument on NASA Aqua/EOS polar orbit satellite is a 2378 channel
173 nadir cross-track scanning infrared spectrometer. It can provide profiles of a number of
174 trace gases, including ozone and CH₄ (Susskind et al., 2003). The footprint of these
175 retrieval data is of 45 km by 45 km and their most sensitive region is in an altitude range
176 of 300-600 hPa. Many studies have shown that these AIRS retrieval constituents are
177 useful indicators for detecting stratospheric intrusions. He et al. [2011] suggested that
178 AIRS can observe the enhanced tropospheric ozone that is of stratospheric origin.
179 Xiong et al. [2013] reported that AIRS is capable of observing abnormal depletion in
180 CH₄ in the troposphere during intrusions. AIRS offers good latitude-longitude coverage.
181 Here we use version 6 of the AIRS Level-3 ozone and methane retrieval products.

182 2.3. Meteorological reanalysis

183 European Centre for Medium-Range Weather Forecasts (ECMWF) reanalysis
184 ERA-interim data are also used. After November 2000 the data are based on the
185 T511L60 version available with a 6-h temporal resolution and $3^\circ \times 3^\circ - 0.125^\circ \times$
186 0.125° latitude-longitude grid (Dee et al., 2011). The dataset from 15 isentropic and
187 37 pressure levels interpolated into $0.5^\circ \times 0.5^\circ$ grid are applied for present study.

188 2.4. HYSPLIT model

189 Backward (forward) trajectories in given starting locations are capable to
190 reproduce the sources (destinations) of the air parcel that will allow us to examine the
191 intrusions of stratospheric origin in the troposphere (e.g. Elbern et al., 1997). The
192 Hybrid Single Particle Lagrangian Integrated Trajectory model (HYSPLIT) developed
193 by the National Oceanic and Atmospheric Administration (NOAA)'s Air Resource
194 Laboratory (ARL) (Rolph, 2003; Stein et al., 2016) is applied to calculate the backward
195 and forward trajectories. The calculation method of the model is a hybrid between the
196 Lagrangian approach and the Eulerian methodology. In this paper, Global Data
197 Assimilation System (GDAS) datasets are adopted for driving the HYSPLIT.
198

199 **3. Results and discussion**

200 3.1. Meteorological synoptic situation

201 On the morning of 29 November 2014, a 500-hPa trough developed on the western
202 side of Lake Baikal (Western Siberia). The trough moved southeastward and extended
203 equatorward and its southern tip separated from the westerlies in the afternoon of 30
204 November 2014 (Fig. 2b), forming a COL near the radar site as shown by the closed
205 geopotential contour. The black stars in Figure 1 and other figures indicate the location
206 of the radar site. On the following days, the COL system moved northeastward
207 gradually (Fig. 2b) and finally stayed over eastern Russia near Sakhalin Island until it
208 reconnected and merged to the westerly flow. 315 K isentropic PV patterns have shown
209 the coarse resolution features of intrusions from the polar reservoir across the
210 tropopause into the midlatitude troposphere. The PV streamer curved and rolled up
211 cyclonically along the western flank of the COL (Fig. 2b).

212 Fig. 3 shows the time series of hourly surface meteorological parameters over the
213 Beijing station. The data are obtained from the Chinese National Meteorology
214 Information Center and is less than 50 km from the MST radar site. As the dry-cold air
215 invasion accompanied with the COL travelled deeply into the planetary boundary layer,
216 it brought severe weather to the surface, including a rapid decrease in temperature and
217 humidity, and rapid increase in surface wind and sea level pressure. The humidity
218 decreased from ~85 to 12 percent within less than 8 hours. It is well established that the
219 polar-type COLs have strong potential to trigger deep convection (Price and Vaughan,
220 1993). To examine the potential convection, maps of high quality Climate Data Record

221 (CDR) of daily Outgoing Longwave Radiation (OLR) are displayed in Fig. 4. During
222 the development of the COL, a local region with abnormal low OLR value was clearly
223 observed near the radar site on 29 November (Fig. 4b). The Satellite-observed cloud
224 top temperature also showed the low values corresponding to the low OLR (figure not
225 shown), indicating that convection may be generated near radar side on 29 November.
226 Please note that we did not observe such low value either in OLR (Fig.4c, d) or in cloud
227 top temperature near the radar side on 30 November and 1 December. The time for all
228 the observations in this paper is shown in Universal Time (UTC) which is eight hours
229 behind Beijing standard time (LT=UTC+8).

230 **3.2. MST radar observations**

231 Radar echo power, horizontal wind vector, vertical wind, and radar aspect
232 sensitivity are plotted in Figure 5 as function of height and time during the passage of
233 the COL. Time variation of RT (black line) and LRT (black crosses) heights are also
234 displayed. The RT height first experienced a rapid descent, and then increased rapidly,
235 forming a deep V-shaped structure of ~4 km depth. The vertical velocity of the RT
236 height variation (both the rapid descent and ascent branches) reaches up to 0.28 km/h.
237 The rapid RT variation in altitude is in fact the response of the tropopause fold below
238 the jet stream, which will be well represented in Fig. 8a. Rapid variation in RT height
239 remained a region with low echo power (marked by R on Fig. 5a) and low aspect
240 sensitivity (marked by R' on Fig. 5d) where they should be normally high value within
241 the 'normal' tropopause layer. Unlike the RT height, the radiosonde LRT altitudes are
242 nearly constant during the COL passage. In normal conditions, RT agrees well with the

243 LRT altitude, such as indicated by Fig. 6a. However, large differences, of order of 2.5
244 km (as shown in Fig. 6b at 12 UTC 30 November), are observed between LRT and RT
245 in altitude during the passage of the COL as expected. It is the difference in definition
246 that contribute most to the large differences, especially under the tropopause fold
247 conditions (e.g. Yamamoto et al., 2003 and Fukao et al., 2003). It is worth noting that,
248 in Fig.6b, although there is no clear reversion in the radiosonde temperature profile
249 within the height of RT, the RT height exactly corresponds well to the reversion of
250 zonal and meridional wind and potential temperature gradient. Such differences
251 between RT and LRT heights can commonly be observed, especially during extreme
252 synoptic situations such as cyclone (e.g. Alexander et al., 2012).

253 The most important observation in this detailed case experiment is the strong
254 downdrafts (hereinafter inferred to as main downdrafts) observed immediately
255 preceding the rapid RT ascent (Fig.5c). The radar echo power sharply weakened (dotted
256 rectangle in Fig.5a) and the wind direction changed rapidly (Fig.5b, change from
257 dominant southerly wind to dominant northerly jet) within the height region of the main
258 downdrafts. As mentioned previously, abnormal low value in OLR and cloud top
259 temperature indicates the possible occurrence of convective activity on 29 November,
260 but nothing special appeared on 30 November near radar site. Consequently, we
261 preliminarily consider that the main downdrafts occurred near 07 UT 30 November
262 might not be produced directly by convective activity. Here, the accurate origin of the
263 main downdrafts will not be discussed in detail, and it is also beyond the scope of
264 present study.

265 The research by Hocking et al. (2007) has suggested that the rapid ascent in RT
266 height ($>0.2 \text{ km h}^{-1}$) can be a valuable **diagnostic** for the occurrence of stratospheric
267 intrusions. Here in this paper, the main downdrafts preceding the rapid RT ascent
268 observed by the Beijing MST radar are thus suspected to be an important feature or
269 response of some form of vertical stratospheric intrusions. Firstly, as the tropopause
270 descends (folded downward), it will displace stratospheric air into the troposphere (e.g.
271 Hoskins et al., 1985). Secondly, the main downdrafts will act as an effective way to
272 weaken the tropopause by means of continuously impinging on the tropopause, through
273 which the stratospheric air is permitted to penetrate down into the free troposphere (e.g.
274 Hirschberg and Fritsch, 1993; Kumar, 2006). In addition, after the main downdrafts,
275 the observed region near the upper troposphere with strong backscatter echoes (marked
276 by Q) and especially with abnormal high aspect sensitivity (marked by Q') may also be
277 a weak signature of the possible intrusions. In normal conditions, they are usually low
278 in value in the upper-troposphere (such as the region marked by P and P'). As we
279 mentioned before, the large value in radar aspect sensitivity is mainly caused by
280 reflection from stable atmospheric layer, such as the tropopause or lower-stratosphere.
281 When stable stratospheric air intrudes into the troposphere and without mixing with the
282 surrounding air mass, the intrusions in the free troposphere will be reflected as abnormal
283 large aspect sensitivity. Further direct evidence of the relevant intrusions in dynamical
284 and chemical aspects will be demonstrated in next section, using satellite AIRS and
285 global reanalysis data.

286 3.3. Associated stratospheric intrusions

287 Due to the sensitivity of the AIRS retrieved ozone and CH₄ is between 300-600
288 hPa. Fig. 7 shows the 500 hPa distribution of AIRS observed ozone and CH₄, along
289 with the AIRS tropopause contour (defined based on the temperature lapse-rate). The
290 ozone distribution maps (left panels of Fig. 7) clearly show a large area with enhanced
291 tropospheric ozone (>80 ppbv) near the radar site during the passage of the COL.
292 Moreover, severe CH₄ depletion (<1840 ppbv) was also observed (right panels in Fig.
293 7). These features of the ozone enhancement, CH₄ depletion, and the corresponding low
294 tropopause altitude clearly support the evidence of vertical downward cross-tropopause
295 stratospheric intrusions on 30 November.

296 The vertical cross-section of ECMWF PV and specific humidity at 1800 UT 30
297 November 2014 and the daily AIRS ozone on 30 November 2014, along a constant
298 latitude 40° N, is shown in Fig. 8. **Please note that the high-PV and dry air have been**
299 **observed intruding deep into troposphere of as low as 650 hPa (~3.6 km). Whereas the**
300 **vertical structure of AIRS ozone has shown that the enhanced ozone intruded into**
301 **troposphere of ~500 hPa. This difference in vertical scale of intrusion between ozone**
302 **and PV parameters is most likely due to two reasons: 1) the local high PV value**
303 **observed near ~600 hPa is not a true stratospheric characterized intrusion but rather**
304 **adiabatically-produced high PV (e.g. Skerlak et al 2015); 2) the relatively poor vertical**
305 **resolution of AIRS ozone data may have limited the refined observation of the**
306 **intrusions. From this figure, however, one thing is clear that stratospheric air (dry**
307 **ozone-rich and high PV) intrusions are indeed occurred and observed (at least intruded**
308 **downward into ~500 hPa).**

309 3.4. Trajectory model analysis

310 Figure 9 shows 30h backward trajectories ending at the radar site at 18 UT 29
311 November (left panel) and at 18 UT 30 November (right panel). As expected, the air
312 masses parcel transported eastward horizontally before the occurrence of main
313 downdrafts (Fig. 9a). Whereas after the downdrafts, the trajectories clearly show
314 downward intrusions originated from the western side of Lake Baikal. Furthermore, a
315 huge dry intrusion is tracked according to the criterion (based on Lagrangian method)
316 in Raveh-Rubin (2017). Trajectory results further support the evidence of **downward**
317 **intrusions** that closely related with the main downdrafts.

318 On the other hand, 30-h forward trajectories starting at 00 UT 30 November (left
319 panel) and 00 UT 1 December (right panel) are shown in Fig. 10. It is interesting to note
320 that, from Fig. 10a before the passage of COL, the air parcels at 4 km transport rapidly
321 upward (by more than 4 km within ~23 h) and northeastward to the upper-troposphere
322 of East Siberian. This upward and poleward transportation is associated with a warm
323 conveyor belt (southerly flows dominate) that is located ahead of the COL. It
324 contributes to transporting the tropospheric moist and polluted air (such as aerosol) into
325 the upper-troposphere and even the lower stratosphere (e.g. Stohl et al., 2003; Sandhya
326 et al., 2015). After the downdrafts, forward trajectories in Fig. 10b demonstrate that the
327 dry intrusion air parcels continue to be transported downward and southeastward to the
328 boundary layer or even the surface.

329 3.5. Strong downdrafts preceding rapid tropopause ascent and discussion

330 Figure 11a shows another 20 typical cases of strong downdrafts preceding rapid

331 RT ascent for the period March 2012 and Jan. 2015 (shown placed end-to-end), the
332 LRT height (plotted in crosses) and the vertical velocity of the RT (plotted in orange
333 line) is also plotted. These cases (marked by black rectangular boxes and labeled as S1,
334 S2, S3..., and S20) are identified based on the following criteria: 1) the amplitude of
335 the RT ascent should exceed 0.6 km (four range gates), 2) vertical velocities of the RT
336 ascent excess 0.1 km/h, 3) the downdrafts occurred preceding the RT ascent should >0.5
337 m/s, and the height region of the downdrafts should pass through the RT layer. The
338 criteria are put forward mainly to avoid the influence of the RT spikes. Figure 11b
339 shows the backward trajectories for the selected 9 cases. Results show clear evidence
340 of downward intrusions corresponding to the associated strong downdrafts. Their
341 sources are mainly from West Siberia (western side of Lake Baikal), except for the case
342 Tr5. Moreover, according to AIRS daily 500 hPa ozone distribution, most of the cases
343 in Figure 11a (except for the cases S14, S15, S16, S17, S20) were associated with
344 significant ozone enhancement, indicating intrusions of stratospheric origin (as shown
345 in Supplementary figure S1). It is important to note that the RT excursion velocity of
346 all the cases is not all above 0.2 km/h and some are lower than this value (e.g. cases
347 S16 and S18). However, some form of stratospheric intrusions was exactly observed in
348 such cases from both the trajectory and satellite results. Therefore, the threshold of
349 vertical velocity of the RT ascent is set at 0.1 km/h, rather than 0.2 km/h (Hocking et
350 al., 2007). Large differences between RT and LRT are also interesting to be noted on
351 some occasions when the RT changes rapidly (such as the occasion near 14 March
352 2012).

353 According to the meteorological chart, the synoptic situation of those cases
354 identified in Fig. 11a are introduced. The cases S1, S2, S8, S9, S10, and S11 seem to
355 have a close relationship with COL development; cases S3, S4, S5, S6, S7, S17, S18,
356 and S19 seem associated with low or high trough systems (at 500 hPa). The remaining
357 cases seem not associated with any significant synoptic development. However, in
358 terms of the distribution of isentropic PV (generally at 315K in winter and 330K in
359 summer), we found that the remaining cases S12, S13, S14, S15, S16, and S20 appear
360 to be associated with some form of stratospheric streamers and their break-up within
361 the previous 48h (not shown). Some cases (e.g. S1 and S2) that appear close on the
362 same day were probably caused by the same system. The characteristics of the 20 cases,
363 including background synoptic condition, vertical velocity of the RT ascent, and 500
364 hPa ozone enhancement, have been summarized in Table 2.

365 In the light of present understanding, the strong downdrafts preceding the rapid
366 RT ascent can serve as an important **diagnostic** for intrusion events, during various
367 synoptic processes in any season. This characteristic will be of great use and play an
368 important role in routine identification of stratospheric intrusions. Considering the
369 duration of such downdrafts, a higher time resolution of radar observations will be more
370 helpful. Present study has shown the duration of the majority downdrafts is generally
371 within 1.5-3 hours. We consider, therefore, that the radar resolution should be best
372 within 1h.

373 Although Hocking et al. (2007) have reported that the rapid tropopause ascent
374 (>0.2 km/h) alone can be a useful diagnostic for potential intrusion events. However,

375 using only the information of RT heights might lead to non-negligible errors, as
376 mentioned above in introduction and according to the observations in Fig. 11.
377 Especially on occasions when the RT ascent is between 0.1-0.2 km/h but the
378 corresponding true intrusions were observed, all such intrusion events will be neglected
379 (maybe ~2 per month, refer to Fig. 12a). Whereas on some occasions when the RT
380 ascent exceeds 0.2 km/h, but without observing true intrusion events (e.g. He et al.,
381 2011), these events will be misdiagnosed (maybe ~13 per month, refer to Fig. 12b). In
382 this sense, using the unique MST radar observations of both the RT height variability
383 and the vertical wind as complementary signature for identifying possible intrusion
384 events is very meaningful.

385 Figure 12 shows four years (2012-2015) of the events with rapid RT ascent (gray
386 bands), and the events with strong downdrafts just preceding the rapid RT ascent (black
387 bands). The identification criteria of such strong downdrafts are similar to that
388 mentioned above and the events are classified according to different value of vertical
389 velocity of the ascent. Among all the events with ascent velocity between 0.1-0.2 km/
390 h, about one-quarter (approximate 2 per month, Fig. 12a) were observed with strong
391 downdrafts preceding them. Whereas, as for the events with the ascent velocity >0.2
392 km/h, the proportion is about a half (approximate 10 per month, Fig. 12b). Here,
393 according to the results above, the occurrence of the strong downdrafts just preceding
394 the rapid RT ascent (black bands in Fig. 12) to a large degree represents the occurrence
395 of possible intrusions. In this way, Fig. 12 indicates that the occurrence of possible
396 intrusions exhibit distinct seasonal variations, with a maximum in winter and spring

397 minimum in summer. This is because the meso- and small-scale atmospheric processes,

398 such as cold air outbreaks, thunderstorms, and convective activities, are more active in

399 winter and spring. They are important sources for downward stratospheric intrusions.

400

401 **4. Conclusions**

402 Detailed case analysis of the cross-tropopause stratospheric intrusions was carried
403 out during a COL. Global reanalysis, satellite data, and HYSPLIT trajectories all
404 showed consistent evidences of dry ozone-rich, high PV, and depleted CH₄ air that have
405 penetrated downward into the free troposphere. The key signature of the stratospheric
406 intrusions in the Beijing MST radar observations is the strong downdrafts just preceding
407 rapid RT ascent. The radar echo power decreased rapidly within the region of strong
408 downdrafts, after which abnormal high aspect sensitivity was recorded in troposphere.
409 Such high aspect sensitivity is served as another potential clue for the intrusions of
410 stratospheric origin.

411 Based on the criteria mentioned in section 3.5, other 20 typical cases of strong
412 downdrafts preceding the rapid RT ascent between March 2012 and January 2015 were
413 presented. These events occurred during different synoptic processes in different
414 seasons. Yet, most of the cases (15 of them) are associated with some form of intrusions
415 observed by combination of AIRS-retrieved ozone and the HYSPLIT trajectory model.
416 Our results show that the radar-derived tropopause height and vertical winds are strong
417 complementary indicators to be used to infer the occurrence of the intrusions of
418 stratospheric origin. This will be of great use and play an important role for the routine
419 identification or prediction of intrusion events. However, the actual origin of the
420 observed downdrafts preceding the rapid RT ascent is not addressed in this paper.
421 Further combination observational experiments need to be conducted, especially
422 combined using ozonesonde soundings, to quantitative analyze the effectiveness of

423 present identification criteria for possible intrusions.

424

425

426 **Acknowledgment**

427 The authors really appreciate Prof Shira Raveh-Rubin for reading and checking the
428 manuscript. This work is funded by National Natural Science Foundation of China
429 (NSFC grants No. 41722404 and 41474132). The authors would like to thanks the
430 technical and scientific staff of Chinese Meridian Space Weather Monitoring Project
431 (CMSWMP) for their support in conducting the experiment. The authors sincerely
432 acknowledge the ECMWF, NASA, and NOAA Air Resources Laboratory (ARL) for
433 providing global reanalysis, satellite trace gases, and HYSPLIT transport model,
434 respectively. The MST radar data for this paper are available at Data Centre for
435 Meridian Space Weather Monitoring Project (<http://159.226.22.74/>). The radiosonde
436 data is available from <http://weather.uwyo.edu/upperair/sounding.html>.

437

438 **References**

- 439 Appenzeller, C., Holton, J. R., & Rosenlof, K. H.: Seasonal variation of mass transport
440 across the tropopause. *Journal of Geophysical Research Atmospheres*, 101(D10),
441 15071–15078, 1996.
- 442 Appenzeller, C., Davies, H. C., & Norton, W. A.: Fragmentation of stratospheric
443 intrusions. *Journal of Geophysical Research Atmospheres*. 101(D1), 1435-1456,
444 1996.
- 445 Alexander, S. P., Murphy, D. J., and Klekociuk, A. R.: High resolution VHF radar
446 measurements of tropopause structure and variability at Davis, Antarctica (69° S,
447 78° E). *Atmospheric Chemistry and Physics*, 13(12), 26173-26205, 2012.
- 448 Bonasoni, P., Evangelisti, F., Bonafe, U., Ravegnani, F., Calzolari, F., Stohl, A., Tositti
449 L., Tubertini O., & Colombo, T.: Stratospheric ozone intrusion episodes recorded
450 at Mt. Cimone during the VOTALP project: case studies. *Atmospheric*
451 *Environment*, 34(9), 1355-1365, 2000.
- 452 Butchart, N., Cionni, I., Eyring, V., Shepherd, T. G., Waugh, D. W., & Akiyoshi, H., et
453 al.: Chemistry-climate model simulations of twenty-first century stratospheric
454 climate and circulation changes. *Journal of Climate*, 23(20), 5349-5374, 2010.
- 455 Chipperfield, M. P., Bekki, S., Dhomse, S., Harris, N., Hassler, B., & Hossaini, R., et
456 al.: Detecting recovery of the stratospheric ozone layer. *Nature*, 549(7671), 211-
457 218, 2017.
- 458 Chen, P.: Isentropic cross-tropopause mass exchange in the extratropics. *Journal of*
459 *Geophysical Research*, 16661-16673, 1995.

460 Chen, G., Cui, X., Chen, F., Zhao, Z., Wang, Y., Yao, Q., ... & Gong, W.: MST Radars
461 of Chinese Meridian Project: System Description and Atmospheric Wind
462 Measurement. *IEEE Transactions on Geoscience and Remote Sensing*, 54(8),
463 4513-4523, 2016.

464 Das, S. S., A. R. Jain, K. K. Kumar, and D. Narayana Rao: Diurnal variability of the
465 tropical tropopause: Significance of VHF radar measurements, *Radio Sci.*, 43,
466 RS6003, doi:10.1029/2008RS003824, 2008.

467 Das, S. S., Ratnam, M. V., Uma, K. N., Patra, A. K., Subrahmanyam, K. V., Girach, I.
468 A., Suneeth K. V. , Kumar K. K., & Ramkumar, G.: Stratospheric intrusion into
469 the troposphere during the tropical cyclone Nilam (2012). *Quarterly Journal of the*
470 *Royal Meteorological Society*, 142(698), 2168-2179, 2012.

471 Das, S.S., M. V. Ratnam, K. N. Uma, K. V. Subrahmanyam, I.A.Girach, A. K. Patra,S.
472 Aneesh, K.V. Suneeth, K. K. Kumar, A.P.Kesarkar, S. Sijikumar and G.
473 RamkuMarch.: Influence of Tropical Cyclones on Tropospheric Ozone: Possible
474 Implications (2016), *Atmospheric Chemistry and Physics*, 16, 4837-4847, 2016.

475 Dee, D. P., Uppala, S. M., Simmons, A. J., Berrisford, P., Poli, P., & Kobayashi, S., et
476 al.: The era-interim reanalysis: configuration and performance of the data
477 assimilation system. *Quarterly Journal of the Royal Meteorological Society*,
478 137(656), 553-597, 2011.

479 Elbern, H., Kowol, J., Sládkovic, R., & Ebel, A.: Deep stratospheric intrusions: a
480 statistical assessment with model guided analyses. *Atmospheric Environment*,
481 31(19), 3207-3226, 2006.

482 Fukao, S., H. Hashiguchi, M. Yamamoto, T. Tsuda, T. Nakamura, M. K. Yamamoto,
483 T. Sato, M. Hagio, and Y. Yabugaki.: Equatorial Atmosphere Radar (EAR).:
484 System description and first results, *Radio Sci.*, 38(3), 1053,
485 doi:10.1029/2002RS002767, 2003.

486 Gage, K. S., & Green, J. L.: Tropopause detection by partial specular reflection with
487 Very-High-Frequency radar. *Science*, 203(4386), 1238-40, 1979.

488 Gerasopoulos, E., Zanis, P., Papastefanou, C., Zerefos, C.S., Ioannidou, A., Wernli, H.:
489 A complex case study of down to the surface intrusions of persistent stratospheric
490 air over the Eastern Mediterranean. *Atmospheric Environment*, 40(22), 4113-4125,
491 2006.

492 Grant, D. D., Fuentes, J. D., Delonge, M. S., Chan, S., Joseph, E., & Kucera, P., et al.:
493 Ozone transport by mesoscale convective storms in western senegal. *Atmospheric*
494 *Environment*, 42(30), 7104-7114, 2008.

495 He, H., Tarasick, D. W., Hocking, W. K., Careysmith, T. K., Rochon, Y. J., Zhang, J., ...
496 & Bourqui, M. S.: Transport analysis of ozone enhancement in Southern Ontario
497 during BAQS-Met. *Atmospheric Chemistry and Physics*, 11(6), 2569-2583, 2011.

498 Hocking, W. K., Careysmith, T., Tarasick, D. W., Argall, P. S., Strong, K., Rochon, Y.
499 J., Zawadzki Irek & Taylor, P. A.: Detection of stratospheric ozone intrusions by
500 windprofiler radars. *Nature*, 450(7167), 281-284, 2007.

501 Holton, J. R., P. H. Haynes, M. E. McIntyre, A. R. Douglass, R. B. Rood, and L. Pfister:
502 Stratosphere-troposphere exchange, *Reviews of Geophysics*, 33(4), 403-439,
503 doi:10.1029/95RG02097, 1995.

504 Hoskins B.J., McIntyre M.E., Robertson A.W.: On the use and significance of
505 isentropic potential vorticity maps. *Quarterly Journal of the Royal Meteorological*
506 *Society*, 111(470), 877-946, 1985.

507 Hirschberg, P. A., and J. M. Fritsch: A study of the development of extratropical
508 cyclones with an analytic model. Part I: The effects of stratospheric structure,
509 *Journal of the Atmospheric Sciences*, 50, 311 –327, doi:10.1175/1520-
510 0469(1993)050<0311:ASOTDO>2.0.CO;2, 1993.

511 Jiang, Y. C., Zhao, T. L., Liu, J., Xu, X., Tan, C. H., Cheng, X. H., ... & Zhao, S. Z.:
512 Why does surface ozone peak before a typhoon landing in southeast China?.
513 *Atmospheric Chemistry and Physics*, 15(23), 13331-13338, 2005.

514 Kim, K. E., Jung, E. S., Campistron, B., & Heo, B. H.: A physical examination of
515 tropopause height and stratospheric air intrusion: a case study. *Journal of the*
516 *Meteorological Society of Japan*, 79(5), 1093-1103, 2001.

517 Kumar, K. K., & Uma, K. N.: High temporal resolution VHF radar observations of
518 stratospheric air intrusions in to the upper troposphere during the passage of a
519 mesoscale convective system over Gadanki (13.5° N, 79.2° E). *Atmospheric*
520 *Chemistry and Physics*, 24(8), 14-17, 2009.

521 Kumar, K. K.: VHF radar observations of convectively generated gravity waves: Some
522 new insights. *Geophysical Research Letters*, 33(1), doi:10.1029/2005GL024109,
523 2006.

524 Leclair de Bellevue J, Baray JL, Baldy S, Ancellet G, Diab R, Ravetta F.: Simulations
525 of stratospheric to tropospheric transport during the tropical cyclone Marlene

526 event. *Atmospheric Environment*. **41**: 6510–6526, 2007.

527 Mahlman, J. D.: Dynamics of transport processes in the upper troposphere. *Science*,
528 276(5315), 1079-1083, 1997.

529 Mihalikova, M., Kirkwood, S., Arnault, J., & Mikhaylova, D.: Observation of a
530 tropopause fold by MARA VHF wind-profiler radar and ozonesonde at Wasa,
531 Antarctica: comparison with ECMWF analysis and a WRF model simulation.
532 *Annales Geophysicae*, 30(9), 1411-1421, 2012.

533 Nastrom, G. D., Green, J. L., Gage, K. S., & Peterson, M. R.: Tropopause folding and
534 the variability of the tropopause height as seen by the flatland VHF radar. *Journal*
535 *of Applied Meteorology*, 28(12), 1271-1281, 1989.

536 Oltmans, S. J., and H. Levy II.: Seasonal cycle of surface ozone over the western North
537 Atlantic, *Nature*, 358, 392–394, 1992.

538 Ottersten, H.: Mean vertical gradient of potential refractive index in turbulent mixing
539 and radar detection of CAT, *Radio Science*, 4, 1247–1249, 1969.

540 Price, J. D., & Vaughan, G.: The potential for stratosphere-troposphere exchange in cut-
541 off-low systems. *Quarterly Journal of the Royal Meteorological Society*, 119(510),
542 343-365, 1993.

543 Rao, T. N., and S. Kirkwood: Characteristics of tropopause folds over Arctic latitudes,
544 *Journal of Geophysical Research*, 110, D18102, doi:10.1029/2004JD005374,
545 2005.

546 Rao, T. N., Arvelius, J., & Kirkwood, S.: Climatology of tropopause folds over a
547 european arctic station (esrange). *Journal of Geophysical Research Atmospheres*,

548 113(D7), 762-770, 2008.

549 Ravindrababu, S., Venkat Ratnam, M., Sunilkumar, S. V., Parameswaran, K., and
550 Krishna Murthy, B. V.: Detection of tropopause altitude using Indian MST radar
551 data and comparison with simultaneous radiosonde observations. *Journal of*
552 *Atmospheric and Solar-Terrestrial Physics*, 121(6), 679-687, 2014.

553 Ramaswamy V, Schwarzkopf MD, Shine KP.: Radiative forcing of climate from
554 halocarbon-induced global stratospheric ozone loss. *Nature* **355**: 810–812, doi:
555 10.1038/355810a0, 1992.

556 Rolph, G.D.: Real-time Environmental Applications and Display sYstem (READY)
557 Website. NOAA Air Resources Laboratory, Silver Spring, MD. [http://](http://www.arl.noaa.gov/ready/hysplit4.html)
558 www.arl.noaa.gov/ready/hysplit4.html, 2003.

559 **Raveh-Rubin, S.: Dry Intrusions: Lagrangian Climatology and Dynamical Impact on**
560 **the Planetary Boundary Layer. *Journal of Climate*, 30(17), 6661–6682, 2017.**

561 Sandhya, M., Sridharan, S., & Indira Devi, M.: Tropical upper tropospheric humidity
562 variations due to potential vorticity intrusions. *Annales Geophysicae*, 33(9), 1081-
563 1089, 2015.

564 **Skerlak, B., Sprenger, M., Pfahl, S., Tyrlis, E., & Wernli, H.: Tropopause folds in ERA-**
565 **Interim: Global climatology and relation to extreme weather events. *Journal of***
566 ***Geophysical Research*, 120(10), 4860-4877, 2015.**

567 Stohl, A., Bonasoni, P., Cristofanelli, P., Collins, W., Feichter, J., & Frank, A., et al.:
568 Stratosphere-troposphere exchange: a review, and what we have learned from
569 staccato. *Journal of Geophysical Research Atmospheres*, 108(D12), 469-474, 2003.

570 Stohl, A., et al.: The influence of stratospheric intrusions on alpine ozone concentrations,
571 Atmospheric Environment, 34, 1323– 1354, 2000.

572 Stohl, A., Wernli, H., James, P., Bourqui, M., Forster, C., & Liniger, M. A., et al.: A new
573 perspective of stratosphere troposphere exchange. Bulletin of the American
574 Meteorological Society, 84(11), 2003.

575 Stein, A. F., Draxler, R. R., Rolph, G. D., Stunder, B. J. B., Cohen, M. D., & Ngan, F.:
576 NOAA's HYSPLIT atmospheric transport and dispersion modeling system. Bulletin
577 of the American Meteorological Society, 96(12), 150504130527006, 2016.

578 Stevenson, D. S., Dentener, F. J., Schultz, M. G., Ellingsen, K., Noije, T. P. C. V., &
579 Wild, O., et al.: Multimodel ensemble simulations of present-day and near-future
580 tropospheric ozone. Journal of Geophysical Research Atmospheres, 111(D8), 263-
581 269, 2006.

582 Sørensen, J. H., and Nielsen, N. W.: Intrusion of stratospheric ozone to the free
583 troposphere through tropopause folds -a case study. Physics and Chemistry of the
584 Earth Part B Hydrology Oceans and Atmosphere, 26(10), 801-806, 2001.

585 Su, L., Yuan, Z., Fung, J. C., & Lau, A. K.: A comparison of HYSPLIT backward
586 trajectories generated from two GDAS datasets. Science of The Total Environment,
587 527-537, 2015.

588 Susskind, J., C. D. Barnett, and J. M. Blaisdell.: Retrieval of atmospheric and surface
589 parameters from AIRS/AMSU/HSB data in the presence of clouds, IEEE
590 Transactions on Geoscience and Remote Sensing, 41(2), 390–409,
591 doi:10.1109/tgrs.2002.808236, 2003.

592 Vaughan, G., Gouget, H., O'Connor, F. M., & Wier, D.: Fine-scale layering on the edge
593 of a stratospheric intrusion. *Atmospheric Environment*, 35(12), 2215–2221, 2001.

594 Wang, C.: New Chains of Space Weather Monitoring Stations in China. *Space Weather-*
595 *the International Journal of Research and Applications*, 8(8), 2010.

596 World Meteorological Organization (WMO): Atmospheric ozone 1985, WMO Global
597 Ozone Res. and Monit. Proj. Rep. 20, Geneva, Switzerland, 1986.

598 Xiong, X., C. Barnet, E. Maddy, S. C. Wofsy, L. Chen, A. Karion, and C. Sweeney.:
599 Detection of methane depletion associated with stratospheric intrusion by
600 atmospheric infrared sounder (AIRS), *Geophysical Research Letters*, 40, 2455–
601 2459, doi:10.1002/grl.50476, 2013.

602 Yamamoto, M., Oyamatsu, M., Horinouchi, T., Hashiguchi, H., & Fukao, S.: High time
603 resolution determination of the tropical tropopause by the Equatorial Atmosphere
604 Radar. *Geophysical Research Letters*, 30(21), 2003.

605

Radar parameter	Value
Transmitted frequency	50 MHz
Antenna array	24×24 3-element Yagi
Antenna gain	33 dB
Transmitter peak power	172.8 kW
Code	16-bit complementary
No. coherent integrations	128
No. FFT points	256
No. spectral average	10
Pulse repetition period	160 μ s
Half power beam width	3.2°
Pulse length	1 μ s
Range resolution	150 m
Temporal resolution	30 min
Off-zenith angle	15°

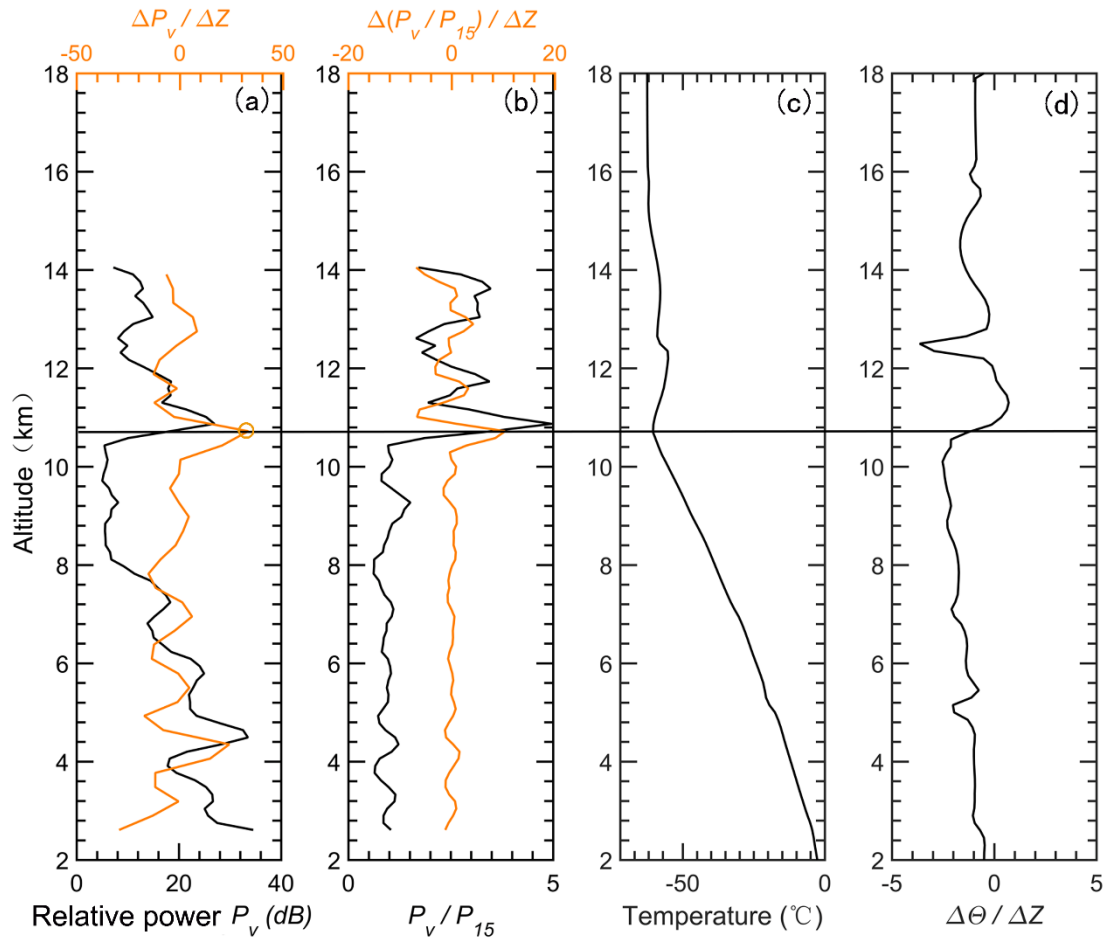
Table 1. Operating parameters in low-mode of the Beijing MST radar.

Cases	Time (year/month/day)	Background condition	Vertical velocity of RT ascent	500 hPa ozone enhancement
S1	2012/03/06	Cut-off low	>0.2 km/h	Enhanced
S2	2012/03/06	Cut-off low	>0.2 km/h	Enhanced
S3	2012/03/12	Low/high trough	>0.2 km/h	Enhanced
S4	2012/03/13	Low/high trough	>0.2 km/h	Enhanced
S5	2012/04/05	Low/high trough	>0.2 km/h	Enhanced
S6	2012/04/05	Low/high trough	>0.2 km/h	Enhanced
S7	2012/04/06	Low/high trough	>0.2 km/h	Enhanced
S8	2012/06/13	Cut-off low	>0.2 km/h	Enhanced
S9	2012/06/13	Cut-off low	>0.2 km/h	Enhanced
S10	2013/08/02	Cut-off low	>0.2 km/h	Enhanced
S11	2013/08/02	Cut-off low	>0.2 km/h	Enhanced
S12	2013/08/03	PV streamer	>0.2 km/h	Enhanced
S13	2013/08/03	PV streamer	>0.2 km/h	Enhanced
S14	2014/01/02	PV streamer	>0.2 km/h	None
S15	2014/01/02	PV streamer	>0.2 km/h	None
S16	2014/01/03	PV streamer	0.1-0.2 km/h	None
S17	2014/01/04	Low/high trough	>0.2 km/h	None
S18	2014/05/02	Low/high trough	0.1-0.2 km/h	Enhanced
S19	2014/05/02	Low/high trough	>0.2 km/h	Enhanced
S20	2015/01/03	PV streamer	>0.2 km/h	None

609 **Table 2.** Characteristics of the 20 cases shown in Fig. 11a.

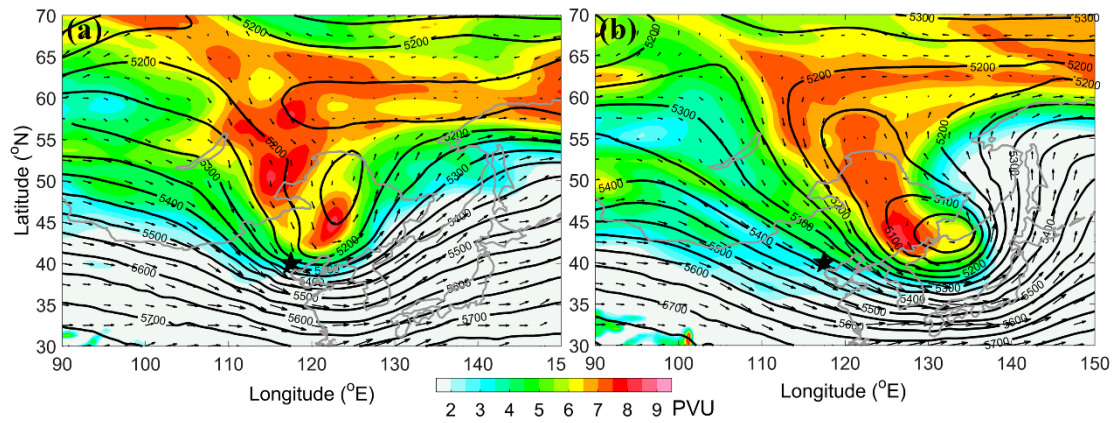
610

611 **Figures**



612

613 **Figure 1.** Example of the vertical height profiles of (a) the relative radar echo power
 614 (black line, smoothed by a 3-point running mean) along with its gradient variation
 615 (orange line), (b) the aspect sensitivity (black line, expressed as the ratio between the
 616 vertical echo power and oblique echo power) along with its gradient variation (orange
 617 line), observed on 12 UT 29 November 2014. The vertical profiles of simultaneous
 618 radiosonde observed temperature and potential temperature gradient are shown in plots
 619 (c) and (d). The black horizontal line denotes the LRT height derived from the
 620 radiosonde temperature profile. The orange circle indicates the RT height derived from
 621 the profile of the radar backscattered echo power.



622

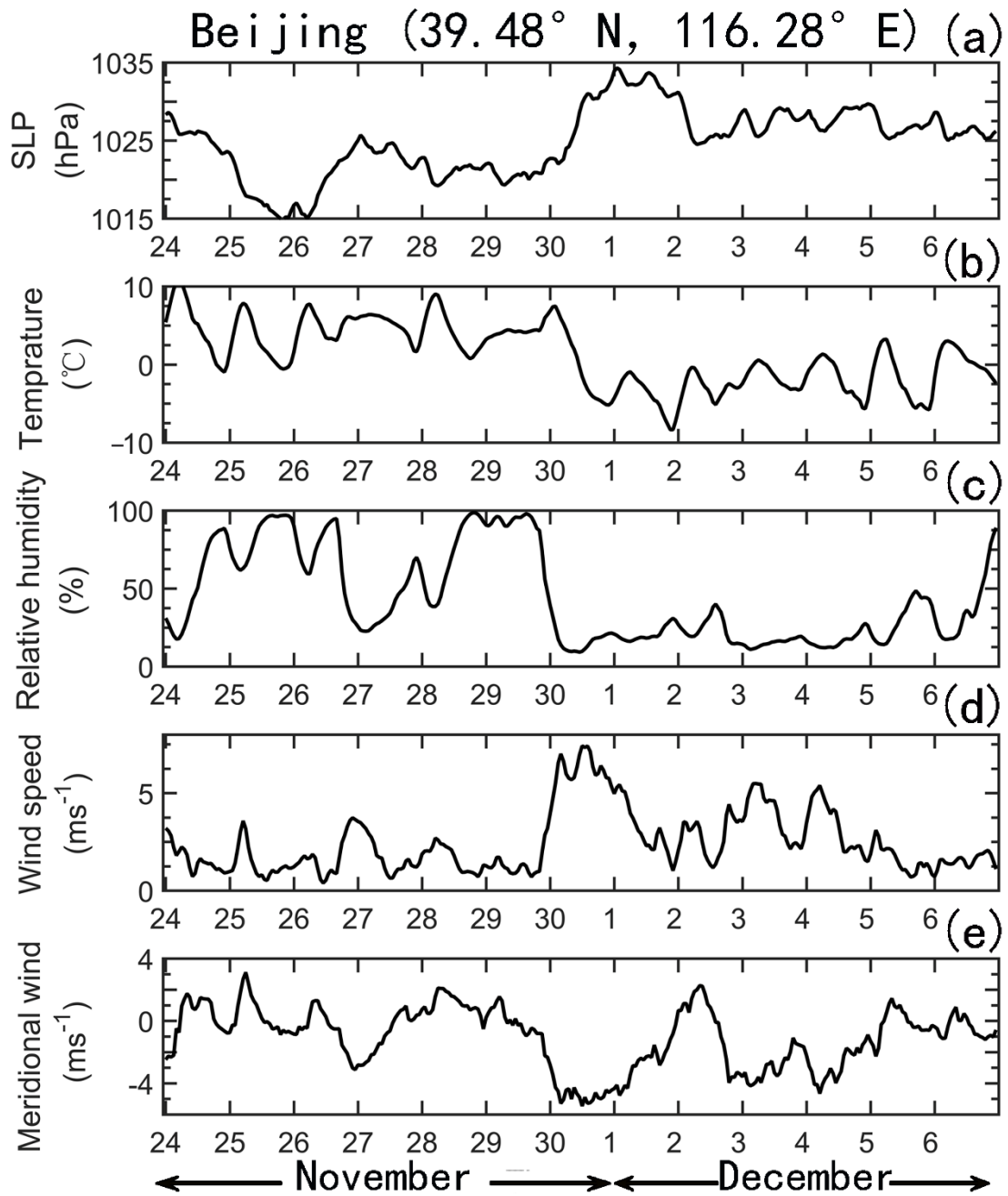
623 **Figure 2.** ECMWF derived isentropic PV map on 315 K surface (shaded above 2 pvu,

624 $1 \text{ PVU} = 10^{-6} \text{ m}^2 \text{ K kg}^{-1} \text{ s}^{-1}$) and geopotential height (contoured every 50 m in solid line)

625 along with the wind vector (arrow) at 500 hPa ($\sim 5.5 \text{ km a.s.l.}$) on (a) 18 UTC 30

626 November 2014, (b) 12 UTC 1 December 2014. The black star shows the location of

627 Xianghe.



628

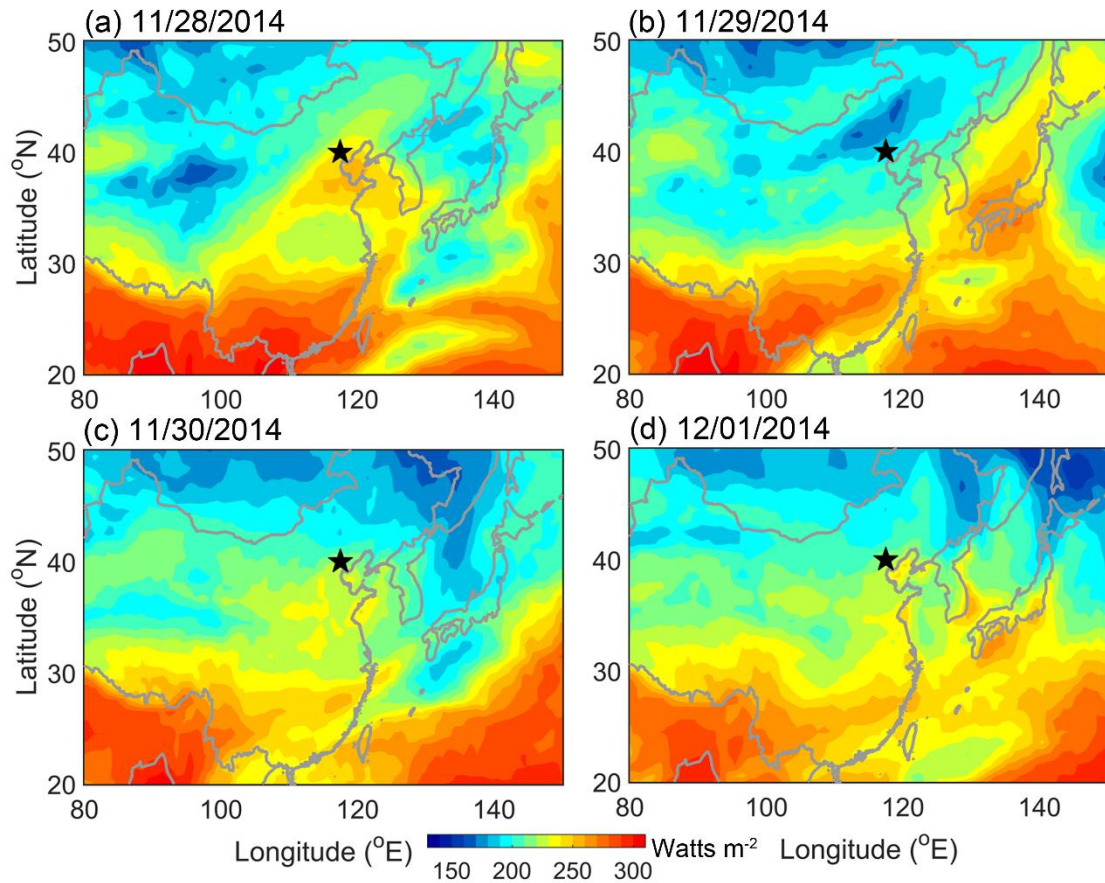
629 **Figure 3.** Time series of surface (~1.2 m above the surface) hourly meteorological

630 measurements of (a) sea level pressure, (b) temperature, (c) relative humidity, (d)

631 horizontal wind, and (e) meridional wind during the period 24 November-6 December

632 2014, observed over the Beijing station (39.4° N, 116.2° E, 31.3 m above sea level).

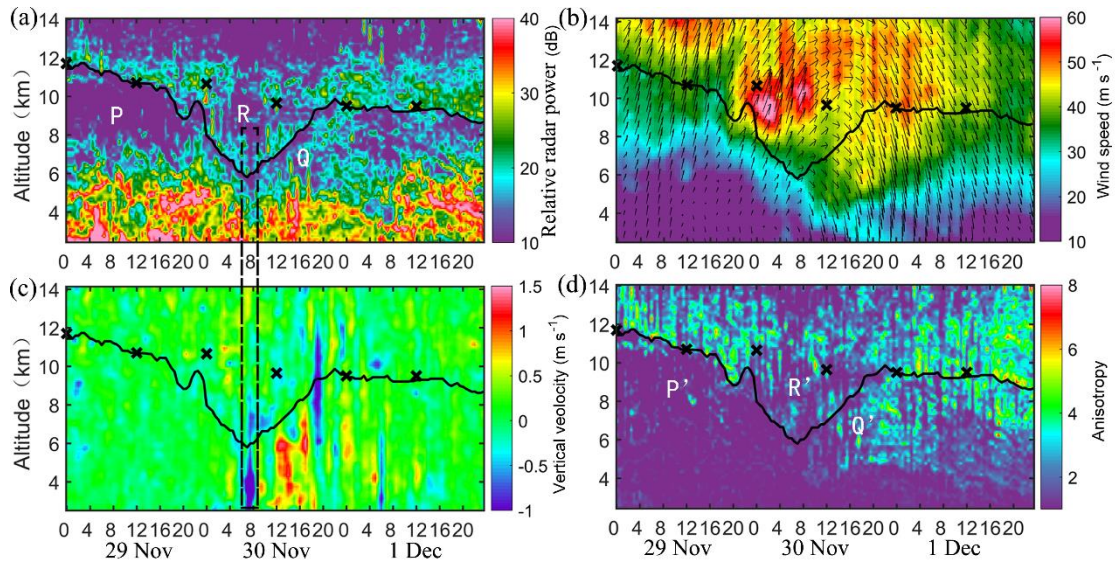
633



634

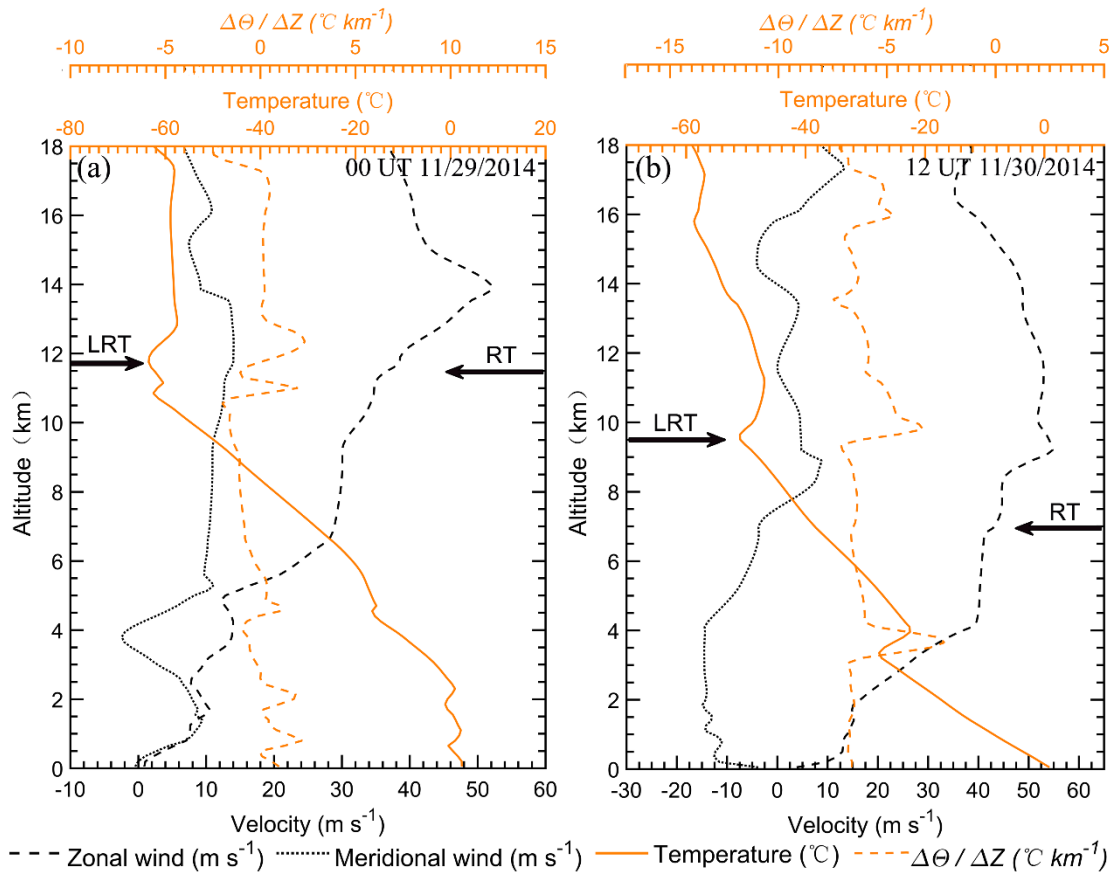
635 **Figure 4.** Contour maps of the high quality Climate Data Record (CDR) of the daily
 636 Outgoing Longwave Radiation (OLR), derived from the NOAA high-resolution
 637 infrared radiation sounder (HIRS) on (a) 28 November, (b) 29 November, (c) 30
 638 November, and (d) 1 December 2014. The black star shows the location of Xianghe.

639

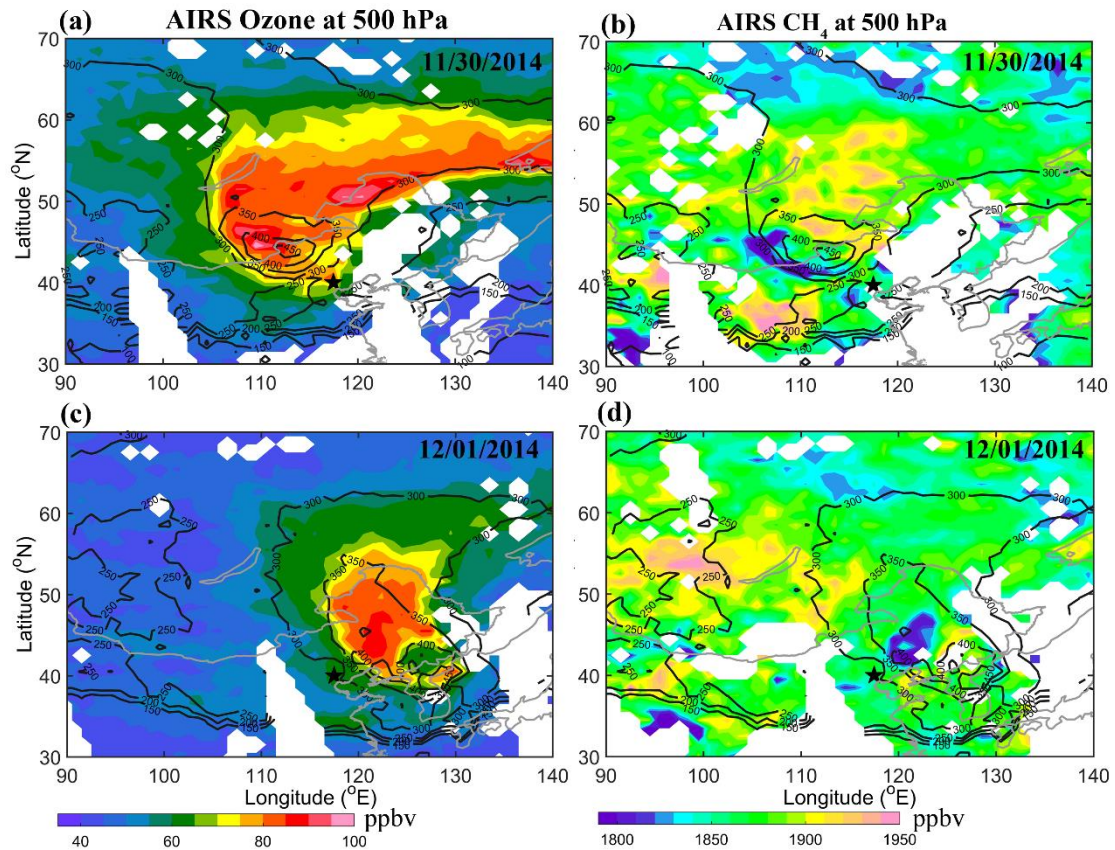


640

641 **Figure 5.** Altitude-time section of (a) the radar backscattered echo power in zenith
 642 direction, (b) the horizontal wind speed along with wind vector, of which the up and
 643 down arrows represent north and south respectively, and left-right is west-east, (c) the
 644 vertical velocity, and (d) the aspect sensitivity, observed by the Beijing MST radar from
 645 29 November to 1 December 2014. The black curve shows the radar-determined
 646 tropopause, as defined in section 2.1. The dotted rectangle highlights the strong
 647 downdrafts immediately preceding the rapid tropopause ascent. The positions of the
 648 LRT tropopause heights, derived from the nearly simultaneous collocated GPS
 649 radiosonde temperature profile, are marked by crosses.



650
 651 **Figure 6.** Vertical profiles of zonal wind, meridional wind, temperature, and potential
 652 temperature gradient derived from the GPS radiosonde measurements, at (a) 0000 UTC
 653 29 November 2014 and (b) 1200 UTC 30 November 2014. The bold arrows on the left
 654 and right side of each panel indicate the radiosonde derived LRT tropopause and radar-
 655 derived tropopause height, respectively.
 656



657

658 **Figure 7.** 500 hPa Ozone (left panels) and methane CH₄ (right panels) distribution

659 along with the tropopause height contour, derived from the AIRS satellite observations.

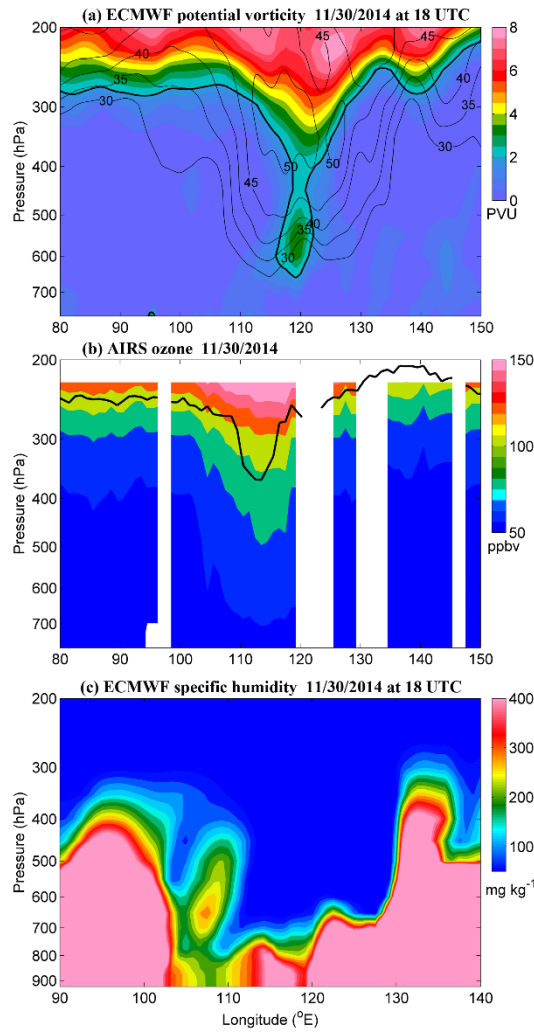
660 The top and bottom plots show the data of 30 November 2014 and 1 December 2014,

661 respectively. According to the Aqua Orbit Tracks (not shown), the time range of the

662 satellite passage is between ~04:00-07:25 on 30 November and between ~03:15-06:35

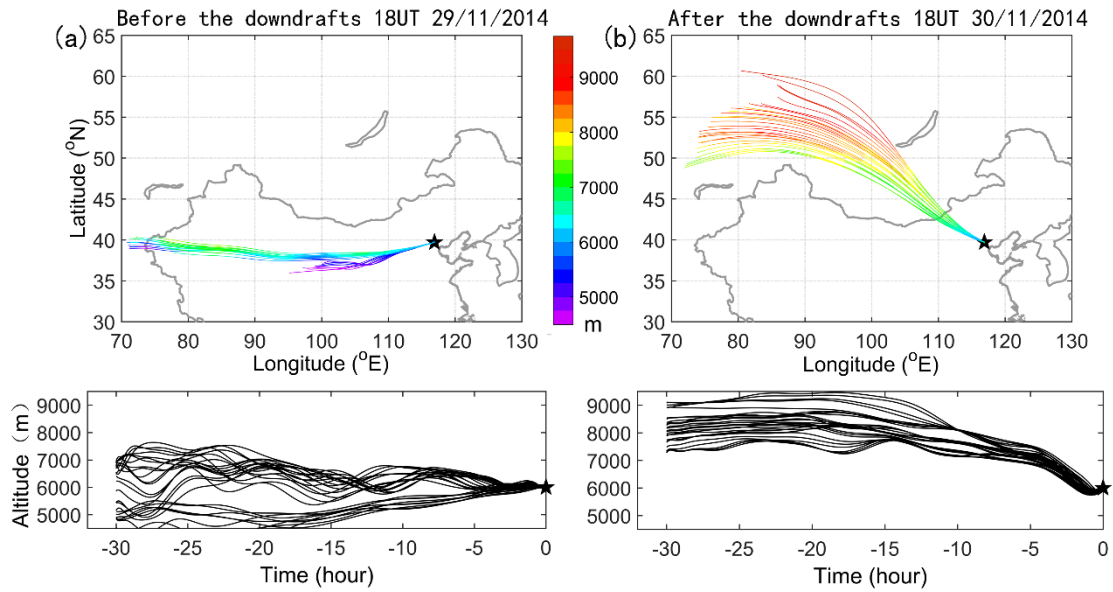
663 on 1 December 2014. The black star indicates the location of Xianghe.

664



665

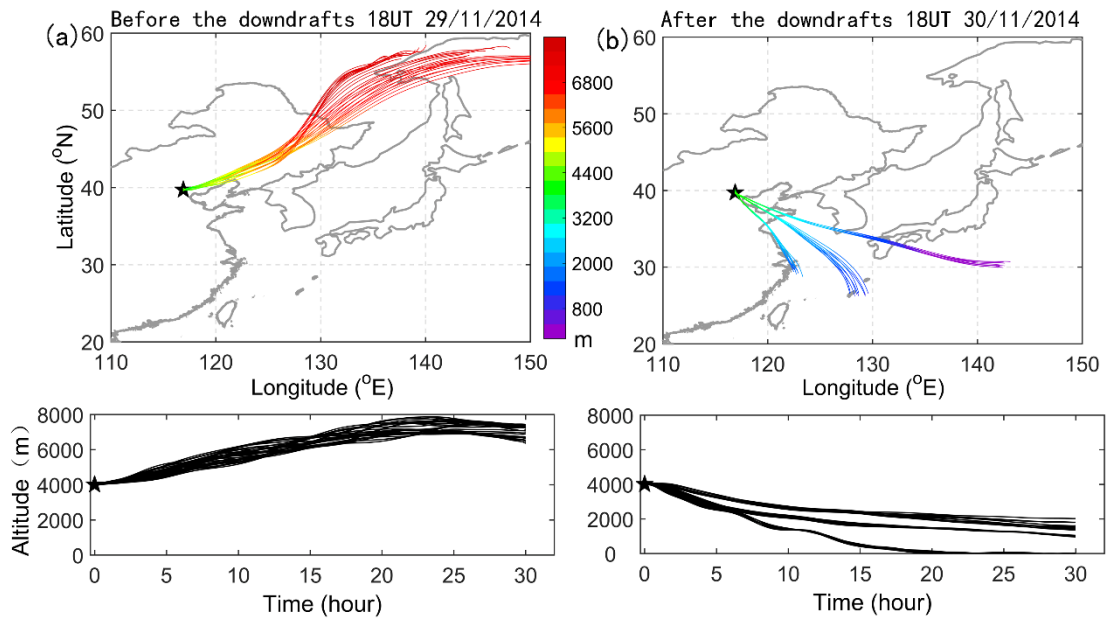
666 **Figure 8.** Longitude-pressure cross section of (a) ECMWF PV (colors, in pvu) along
 667 with horizontal wind contour (thin black line, m/s) at 18 UTC on 30 November 2014,
 668 (b) AIRS ozone mixing ratio (colors, in ppbv) along with tropopause height (black line)
 669 on 30 November 2014, and (c) ECMWF specific humidity (colors, in mg kg^{-1}) at 18
 670 UTC on 30 November 2014, at a constant latitude 40° N (nearest grid point in the
 671 latitude of Xianghe). The bold line in (a) marks the isotropic line of PV at 2 pvu.



672

673 **Figure 9.** Illustration of 30 h three-dimensional backward trajectories ending at
 674 Xianghe at 6000 m using National Oceanic Atmospheric Administration (NOAA)
 675 HYSPLIT model: (a) before the main downdrafts at 18 UTC on 29 November 2014,
 676 and (b) after the main downdrafts at 18 UTC on 30 November 2014. The HYSPLIT
 677 ensemble consists of 27 trajectories. Upper plots show the horizontal projection of the
 678 trajectories, and the lower plots show the corresponding time-height vertical
 679 displacement of the trajectories.

680

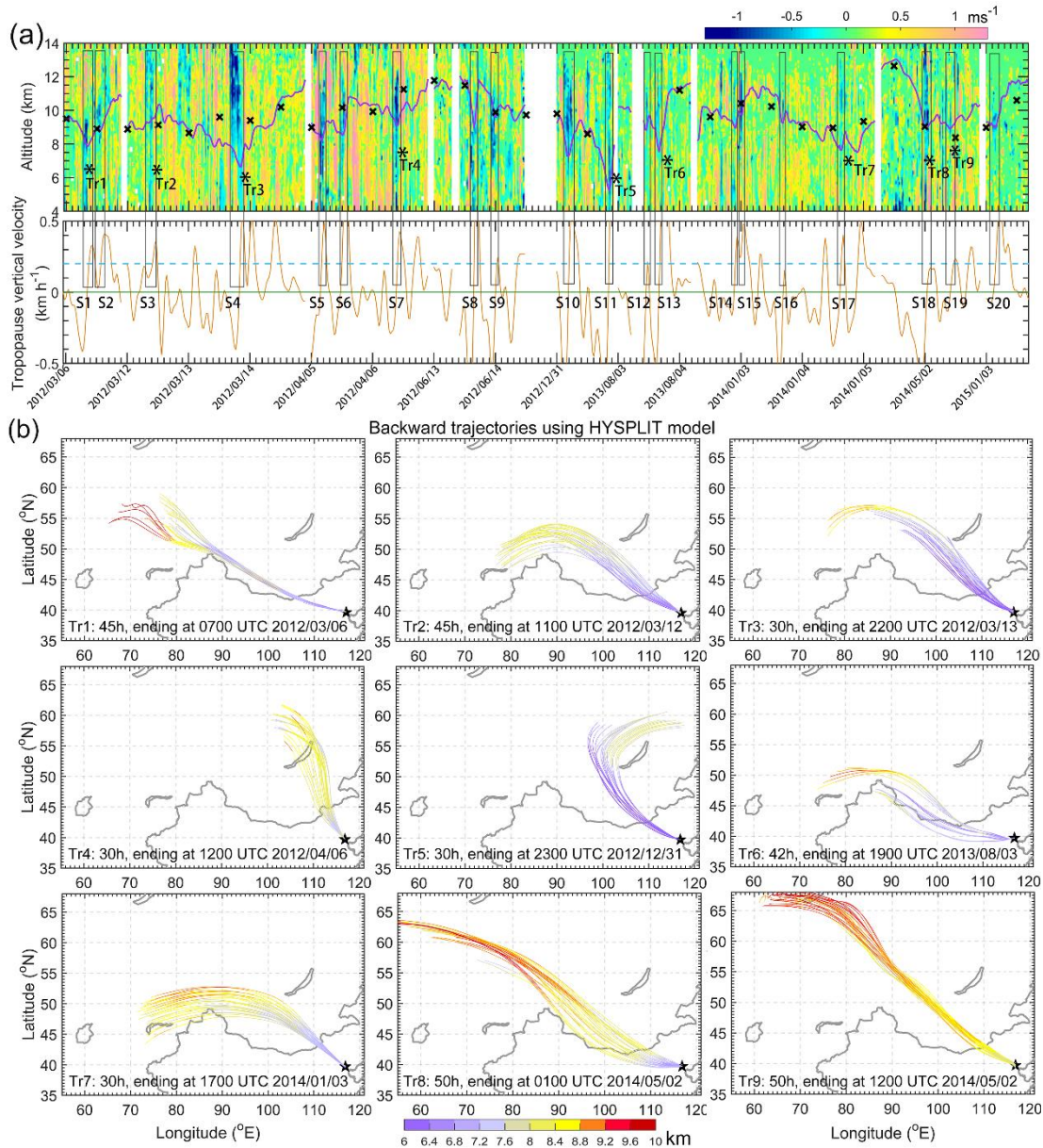


681

682 **Figure 10.** Same as Fig.10 but for three-dimensional forward trajectories starting at

683 Xianghe at 4000 m: (a) before the main downdrafts at 00 UTC on 30 November 2014,

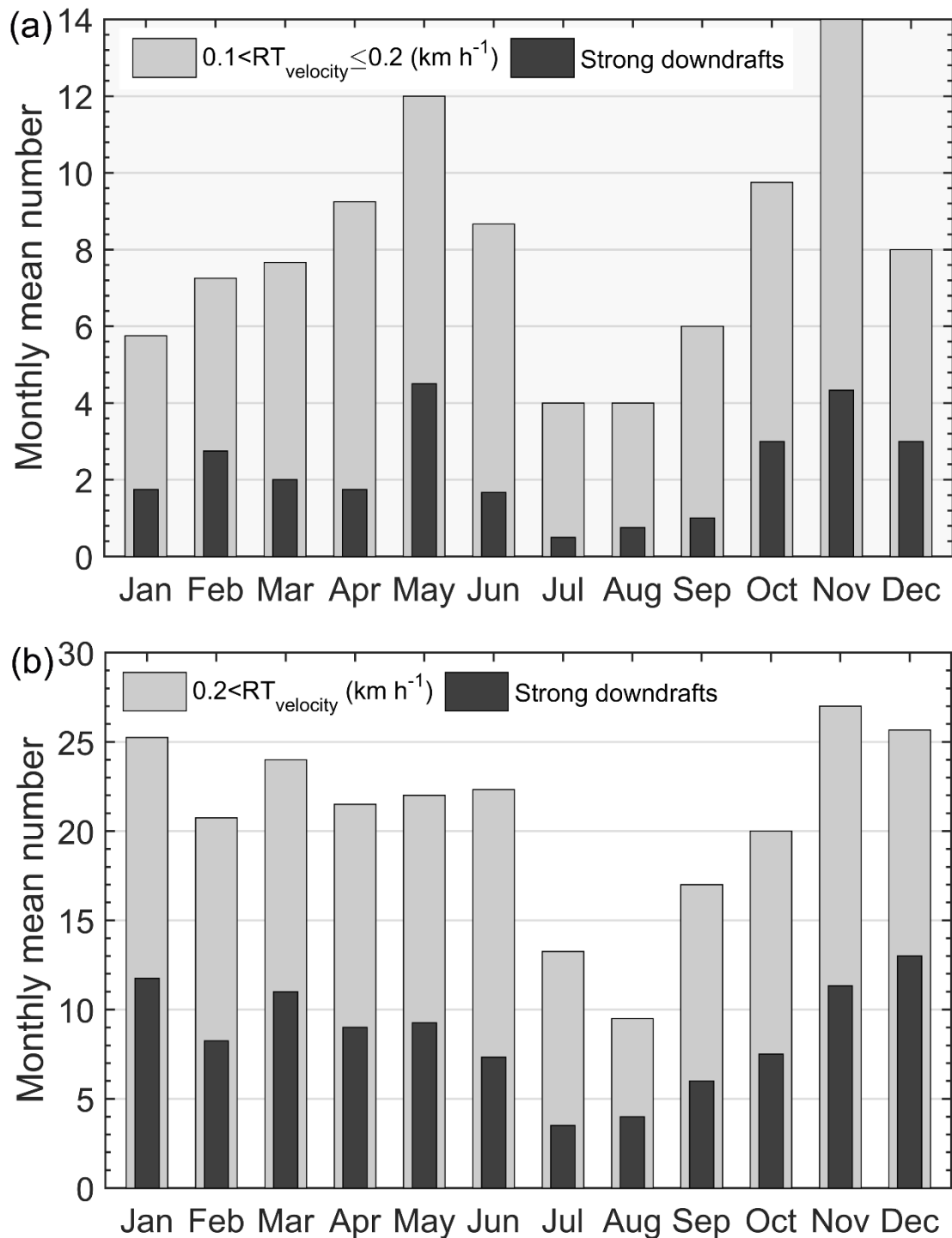
684 and (b) after the main downdrafts at 00 UTC on 1 December 2014.



685

686 **Figure 11.** (a) Height-time section of several episodic observations of the radar-derived
 687 vertical wind (colors in m/s) along with RT height (purple bold line) and LRT height
 688 (bold crosses), between March 2012 and Jan. 2015. The corresponding vertical velocity
 689 of the RT (orange line) is plotted in the lower panel of (a), dotted blue line indicates the
 690 value of 0.2 km/h. Dates for the observations are displayed as year/month/day. Black
 691 rectangular boxes represent the cases of strong downdraughts (absolute value ≥ 0.5 m/s)
 692 preceding rapid tropopause ascent (>0.1 km h⁻¹) and are labeled as S1, S2, S3..., S20.

693 Symbol ‘*’ labeled as Tr1-Tr9 indicates the ending point of the corresponding
694 trajectories in Fig.12b. (b) Results of backward trajectories (colors in km) of the typical
695 9 selecting cases from Fig.12a, providing the signature and source of possible
696 stratospheric intrusions.
697



698

699 **Figure 12.** Four years (2012-2015) of radar-determined monthly mean number of rapid

700 tropopause ascent (gray bands) and the corresponding strong downdrafts just preceding

701 the rapid tropopause ascent (black bands). (a) Gray bands: with the ascent by at least

702 0.6 km and the excursion velocity is between 0.1-0.2 km h⁻¹; black bands: except for

703 the criteria of gray bands, strong downdrafts occurred preceding the rapid RT ascent

704 must exceed 0.5 m s^{-1} and pass through the RT layer. (b) Same as (a) but for the
705 occasions when the ascent velocity is larger than 0.2 km h^{-1} . According to the study
706 here, the black bands in the histogram well represent the occurrence of possible
707 stratospheric intrusions.

708